Research Article

Holocene hydroclimate and dust activity, as reconstructed from the sediments of Lake Bayanchagan, on the northern margin of the East Asian summer monsoon

Wubiao Li[1,2], Wenying Jiang[1], Shiling Yang[1,2], Jie Lin[1,2] and Yujie Wang[1,2]

[1]Key Laboratory of Cenozoic Geology and Environment, Institute of Geology and Geophysics, Chinese Academy of Sciences, Beijing 100029, China and [2]College of Earth and Planetary Sciences, University of Chinese Academy of Sciences, Beijing 100049, China

Abstract

The sediments of closed-basin lakes on the margin of the East Asian summer monsoon (EASM) are valuable archives of past changes in hydroclimate and dust activity and thus potentially can help us to understand future climate changes. We present high-resolution, well-dated records of the grain size and carbonate mineralogy from Lake Bayanchagan, northern China, spanning the last 11.5 ka. Grain-size endmember (EM) analysis distinguished four EMs, each linked to different sediment transport processes. EM1 (0.4–0.6 µm) and EM3 (14–102 µm) reflect the strength of regional dust activity, whereas EM2 (1.3–31 µm) represents variations in local hydrodynamic conditions related to lake-level changes and EM4 (68–500 µm) is associated with local dust activity. Our results show that a high lake level and weakened dust activity occurred during 10–5.8 ka, as indicated by increased EM2 and decreased EM3, respectively. After 5.8 ka, EM2 decreased as the three other EMs increased, and dolomite appeared in the sediments while calcite decreased—indicating both a decline in lake level and strengthened dust activity. The fluctuations in lake level and dust activity are in good agreement with precipitation variations reconstructed from other records, which are in turn correlated to movement of the EASM rainfall belt, in response to temperature changes.

Keywords: Holocene, East Asian summer monsoon, Grain size, Carbonate, Lake level, Dust activity

(Received 5 March 2023; accepted 12 September 2023)

INTRODUCTION

Northern China is located in the transition between arid and sub-humid climatic zones, within the arable–pastoral ecotone. Changes in hydroclimate, mainly controlled by the East Asian summer monsoon (EASM), present significant challenges to the management of freshwater resources and the food security of this region. Thus, the formulation of plans for domestic and agricultural water use and an assessment of the possible impacts of global climate change on the hydroclimate of northern China are urgently needed. Previous research has shown that increased global temperatures may lead to higher temperatures and drought events in northern China (Zhang et al., 2020), which would accelerate the drying of lakes. Evaporation from the lakes is estimated to increase by ∼17.7% annually by the end of this century (Wang et al., 2018). This scenario is consistent with the prediction of Held and Soden (2006) that Earth's dry regions will experience intensifying droughts with ongoing global warming. However, others have argued that future temperature rises of 2–3°C in SE Asia could lead to a northward shift of the EASM rainfall belt and subsequent increased precipitation in northern China (Yang et al., 2015; Huang et al., 2021). Thus, the nature of the

hydroclimatic response of northern China to ongoing global warming remains controversial.

The global mean temperature during the mid-Holocene, the most recent major warm period, was 0.7–2°C higher than today (Marcott et al., 2013; Shi et al., 2021), and thus the climate of this interval is a potential analogue for future warming (Renssen et al., 2012). In northern China, loess deposits were mainly derived from nearby arid and semiarid regions (Liu, 1985). The grain-size distribution (GSD) of loess is principally controlled by the source-to-sink distance, that is, generally speaking, the greater the dust transport distance, the finer the grain size for dust deposit (Yang and Ding, 2004, 2008; Ding et al., 2005).Therefore, loess grain size is an effective proxy for reconstructing the source–sink distances and, for this study, desert margin migrations associated with the movement of the EASM rainfall belt (Ding et al., 2005; Yang and Ding, 2008; Li et al., 2019). Chinese loess is mainly composed of loosely cemented silt (Liu, 1985), which is vulnerable to erosion, especially during the Holocene (Yang and Ding, 2008; Chen et al., 2013; Qiang et al., 2014). Sediments preserved in lakes in downwind, semiarid regions provide a continuous record of regional eolian activity (Qiang et al., 2014; Chen et al., 2020). However, lake sediments represent a mixture of materials from different sources, reworked and sorted by hydrodynamic processes within the lake proper (Håkanson and Jansson, 1983; Talbot and Allen, 1996), resulting in polymodal GSDs. These sediments represent challenges to partitioning out the eolian component. A recently developed grain-

size endmember (EM) model can help unmix GSD data into the constituent components (Paterson and Heslop 2015). This model has been successfully applied in the reconstructions of sediment provenance, depositional regimes/processes, and paleoclimate in the Tibetan Plateau, Central Asia, and East Africa (Meyer et al., 2013, 2020; Dietze et al., 2014; Liu et al., 2016; Zhou et al., 2019).

Many of the closed-basin lakes on the northern margin of the EASM (Fig. 1) are very sensitive to hydrological changes, because their water input is mainly from monsoonal rainfall, and thus their sediments are valuable archives for determining the paleohydrology and paleoclimate of this region (An et al., 2000; Li et al., 2020). In this study, we analyzed the GSDs and carbonate mineralogy of the sediments of Lake Bayanchagan, with the aim of reconstructing changes in lake level and dust activity during the Holocene, focusing on the hydroclimatic response of northern China to the most recent period of major global warming.

MATERIALS AND METHODS

Lake Bayanchagan (41.64°N, 115.21°E, 1355 m above sea level) is located in the transition between desert and steppe environments in northern China (Fig. 1). The lake is almost completely dry at present, due to human activity, although small shallow areas of water are maintained by summer rainfall. The clastic sediments in Lake Bayanchagan are mainly derived from eolian deposits and runoff-transported materials from the catchment. The present-day climate is mainly controlled by the East Asian monsoon, which comprises two seasonally alternating atmospheric circulations. In winter, a northwesterly dry, cold air mass from Siberia leads to cold and dry weather, while in summer, a southeasterly air mass transports heat and moisture inland from the low-latitude oceans. The mean annual temperature and the mean temperature in January and July are 3°C, −16°C, and 17°C, respectively. The annual precipitation is ~350 mm, ~70% of which falls in summer (June to September).

A sediment core (BY) was collected from a trench area in the center of Lake Bayanchagan. Details of the sedimentary lithology, results of ^{14}C dating, and the pollen stratigraphy of this core are presented elsewhere (Jiang et al., 2006). Two dates from *Potamogeton* seeds in the core were excluded, as some species of this aquatic plant have submerged leaves, and hence subaquatic photosynthesis might introduce a hard-water error into any subsequent ^{14}C date (Törnqvist et al. 1992). A sample of the total organic carbon content of the uppermost sediments (0–2 cm depth) had a ^{14}C age of 570 yr (Table 1). This date, older than the actual age, is likely caused by the influx of "old carbon" to the lake from the catchment or by coastal erosion (Olsson, 2009; Hou et al., 2012). This radiocarbon reservoir age of Lake Bayanchagan is approximately consistent with those of Lakes Hulun (685 yr; Wen et al., 2010), Dali (611 yr; Xiao et al., 2009), and Daihai (360 yr; Peng et al., 2005) in the northern margin of the EASM. To establish an age–depth model, we assumed that the proportion of "old carbon" was relatively constant throughout the core. The reservoir age of 570 yr was subtracted from all the original ^{14}C ages, and the resulting ages were then converted to calibrated ages using the IntCal 20 calibration curve (Stuiver et al., 2020; Fig. 2).

The GSDs of 90 samples, taken at 2 cm intervals, were measured with a Mastersizer 3000 (Malvern Panalytical, UK). Before the measurements were made, all samples were treated with 30% H_2O_2 and then with 10% HCl to remove organic matter and carbonate, respectively, after which 10% $(NaPO_3)_6$ was added,

and the samples were treated with ultrasound for 10 min to promote dispersion. The average GSDs, determined by three repeated measurements for each sample, were used as input data for subsequent calculations. The resulting GSD data set was mathematically decomposed using the AnalySize modeling algorithm developed by Paterson and Heslop (2015). This method aims to establish a physical mixing model that transforms the measured GSDs into a limited number of nonnegative and unimodal grain-size EMs that can be interpreted individually (Meyer et al., 2020).

The carbonate mineralogy of 30 samples from the core was analyzed by X-ray diffraction (XRD; RINT2000 Wide-angle goniometer).

RESULTS

GSDs

During 11.5–10 ka (180–142 cm) (Fig. 3a), the median grain size (Md) varied from 203.4 to 5.8 μm. Most of the samples have trimodal GSDs, with a principal mode at 7.8 μm and two secondary modes at 38 and 0.448 μm. Samples from the depths of 180, 178, 160, 158, 152, and 148 cm have multimodal distributions, with the principal mode between 100 and 609 μm. For example, the GSDs of the samples from the depths of 152 and 148 cm show a major peak at ~410 μm and four minor peaks at 0.448, 7.8, 38, and 152 μm (Fig. 3a). The samples at 160 and 158 cm are roughly bimodal, with the principal mode at ~124 μm and secondary modes at 226 and 410 μm. During 10–5.8 ka (142–46 cm) (Fig. 3b), Md varied between 19.1 and 4.2 μm. The samples have relatively consistent bimodal GSDs, with the major peak at 7.8 μm and a minor peak at 38 μm. During 5.8–0 ka (46–0 cm) (Fig. 3c), Md varied from 39.2 to 4.5 μm, and all the samples have trimodal GSDs, in most cases with the main peak at 7.8 μm and two minor peaks at ~38 and 0.448 μm.

On the C–M plot of grain-size data, where C and M indicate the coarsest percentile (the value at 99%) and the median (the value at 50%) of the GSDs, respectively, three transport mechanisms can be partitioned according to the combination of C and M values, that is, suspension and rolling, uniform suspension, and pelagic suspension (Passega, 1964; Fig. 3d). A C–M plot of the grain-size data from core BY reveals three main groupings (Fig. 3d). The sediments from the depth interval of 180–142 cm fall within all three groups, while those from the intervals of 142–46 and 46–0 cm mainly fall within the pelagic suspension and uniform suspension fields, respectively (Fig. 3d).

EM modeling

The goodness-of-fit statistics show an increasingly better fit (higher R^2) to the raw GSD spectra as the number of EMs increases (Fig. 4a). Thus, we chose a model with four EMs, which explains more than 92% of the variance in the GSDs (Fig. 4a). All EMs have unimodal distributions (Fig. 4b). The modeled peaks of these EMs are ~0.448 μm (EM1), ~7.8 μm (EM2), 38 μm (EM3), and 152 μm (EM4), representing the four major modes—at 0.448, 7.8, 38, and 100–410 μm—indicated by the entire GSD data set (Fig. 4b).

During 11.5–10.2 ka, EM1 values fluctuated between 0.3% and 7.1%. During 10.2–5.8 ka, the proportion of EM1 was very low, averaging at 1.66%, except for two short pulses at 7.9 ka and 6.9 ka. The fluctuations of EM1 increased during 5.8–3.3 ka, followed by a decrease after 3.3 ka.
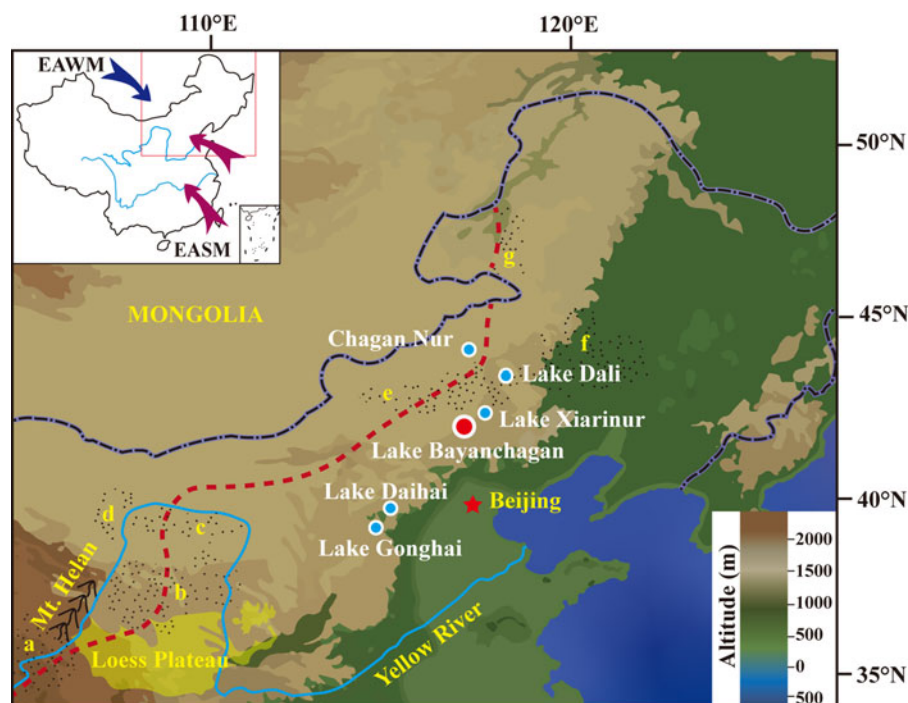
Figure 1. The locations of Lake Bayanchagan and other sites referenced in the text. Also shown are the major deserts of northern China: (**a**) Tengger Desert, (**b**) Mu Us Desert, (**c**) Hobq Desert, (**d**) Ulan Buh Desert, (**e**) Otindag Sandy Land, (**f**) Horqin Sandy Land, and (**g**) Hulun Buir Sandy Land (modified after Yang and Ding, 2008). The red dashed line indicates the modern summer monsoon boundary (Yang et al., 2019), and the arrows indicate the modern trajectory of the East Asian summer monsoon (EASM) (red) and the East Asian winter monsoon (EAWM) (blue).

During 11.5–11.3 ka, EM2 increased from 26% to 98%, followed by a rapid decrease to 5% during 11.3–10.8 ka and an increase to ∼60% during 10.8–10.0 ka. During 10.0–5.8 ka, the relative dominance of EM1 was relatively high (>79%), while subsequently, during 5.8–0 ka, its values fluctuated with a decreasing trend.

The proportion of EM3 was very low before 5.8 ka, except for two periods during 11.3–9.5 ka and during 8–6.3 ka. After 5.8 ka, its values fluctuated with an increasing trend (mean ∼33.6%). The proportion of EM4 fluctuated between 90% and 0% during 11.5–10.8 ka. It was almost absent during 10.8–5 ka and then increased slightly after 5 ka.

Carbonate mineralogy

The XRD results (Fig. 5) show that during 11.5–5.8 ka, calcite dominated the carbonate fraction, with the average content of 47% and the maximum occurring during 10–5.8 ka, during which time dolomite was not detected. During 5.8–4.4 ka, dolomite content increased rapidly to ∼30%, at the expense of calcite. During 4.4–1.8 ka, minor fluctuations occurred in both calcite and dolomite content, while after 1.8 ka, dolomite content decreased and calcite content increased.

DISCUSSION

Holocene changes in lake level and precipitation on the northern margin of the EASM

Clastic materials from different sources get deposited in the lake and are then reworked and sorted by hydrodynamic processes within the lake itself (Håkanson and Jansson, 1983; Talbot and Allen, 1996). Coarse particles tend to be deposited in the nearshore zone, while fine-grained sediments are more common in the deeper waters (Lerman, 1978; Dietze et al., 2014). Investigations of 68 lakes in the marginal zone of the EASM

have confirmed this relationship between lake water depth and sediment grain size (Guo et al., 2016). As shown in Figure 4c, the sediment grain size gradually decreases from 170–500 μm in the nearshore zone to 17–150 μm in the transitional zone, and finally to 2–70 μm in the lake center (Guo et al., 2016).

EM2 represents the relatively fine particle fraction in the Lake Bayanchagan sediments, with a mean grain size of 6.9 μm (90% within the range of 1.3–31 μm) (Fig. 4b). The dominant grain sizes of EM2 are consistent with the offshore-suspension component of sediments in the lake center, as indicated by previous investigations (Xiao et al., 2009; Guo et al., 2016; Fig. 4d). Therefore, EM2 dominates the clastic component of the profundal sediments in Lake Bayanchagan, and it is a proxy for past lake-level changes. The record of EM2 in core BY indicates that the level of Lake Bayanchagan gradually increased during 10.8–10.0 ka and reached a high stand during 10–5.8 ka. Lake levels decreased after 5.8 ka (Fig. 5).

The high stand of Lake Bayanchagan during ∼10–5.8 ka is supported by the C–M plot for core BY, which illustrates that sediment transport is linked to hydrodynamic conditions (Passega, 1964; Bravard et al., 2014). As shown in Figure 3d, the GSDs of sediments in the lower part of core BY (180–142 cm, 11.5–10 ka) are distributed within three zones, suggesting that the hydrodynamic conditions fluctuated substantially during this interval. The GSDs of the sediments in the middle part of the core (142–46 cm, 10–5.8 ka) are distributed mainly in the lower left part of the graph, in the pelagic suspension zone, with the C values of most samples <100 μm, indicating weak hydrodynamic conditions related to a high stand of Lake Bayanchagan. The samples from the upper part of the core (46–0 cm, 5.8 ka to the present) are concentrated in the left-central part of the suspension zone, with C values >100 μm, reflecting a relatively strong hydrodynamic environment due to the lowered lake levels.

Precipitation of lacustrine carbonate is primarily determined by the salinity and Mg/Ca ratio of the lake water (Müller et al., 1972). As salinity increases, calcite precipitates first, followed by

Table 1. Accelerator mass spectrometry dating results for core BY from Lake Bayanchagan, northern China

Depth (cm)	Materials	[14]C age (yr BP)[a]	2σ calibrated range (cal yr BP)[b]	Lab. reference[c]
0–2	Total organic carbon (TOC)	570 ± 50	510–624	GifA-102468
34–36	TOC	3570 ± 60	3002–3353	GifA-102467
40–42	TOC	3830 ± 70	3356–3641	GifA-40002/SMAC-506
46–48	TOC	5270 ± 50	5319–5484	GifA-40001/SMAC-505
76–78	TOC	7040 ± 80	7254–7512	GifA-102466
148–150	TOC	9760 ± 130	10,121–10,732	GifA-102462
148–150	*Potamogeton seeds*	10,800 ± 100	11,604–12,473	GifA-102619
178–180	TOC	10,500 ± 140	11,087–11,935	GifA-102464
178–180	*Potamogeton seeds*	12,030 ± 110	13,158–13,507	GifA-102463

[a]Jiang et al. (2006).
[b]CALIB rev. 8 (Stuiver and Reimer, 1993; http://calib.org)
[c]GifA: the LSCE-UMR CEA/CNRS 1572 (Gif-sur-Yvette, France) for sample preparations and UMS2004 (Gif-sur-Yvette, France) for physical measurements.

aragonite and dolomite (Shapley et al., 2005). This scenario is consistent with an investigation of modern lakes in northern China, which showed that lake water salinity and Mg/Ca ratios increase with decreasing precipitation. As a result, calcite precipitates first, followed by dolomite, and then finally by gypsum and halite (Gu et al., 2015). In core BY, the increase in dolomite at the expense of calcite during 5.8–4.6 ka provides depositional evidence for the salinization of the lake (Fig. 5), indicative of decreasing precipitation and increasing aridity at the study area. This finding agrees with the stable oxygen isotopic composition of authigenic carbonate in core BY. The oxygen isotopic composition of carbonate is mainly controlled by the $\delta^{18}O$ of the lake water, namely the balance between precipitation and evaporation (Leng and Marshall, 2004). Increased monsoonal precipitation results in lower water $\delta^{18}O$ values, whereas evaporation results in higher values (Leng and Marshall, 2004; Yang et al., 2012). The carbonate $\delta^{18}O$ record of core BY suggests enhanced monsoonal precipitation during 10.1–5.8 ka, followed by a large reduction during 5.8–4.6 ka (Jiang and Liu, 2007). The similarity between the carbonate $\delta^{18}O$ and EM1 records, together with the variations of the calcite and dolomite content (Fig. 5), indicate that fluctuations in the lake level of Lake Bayanchagan over the

Holocene were closely linked to changes in monsoonal precipitation.

High lake levels during the Early and Middle Holocene have also been observed in records from other closed-basin lakes on the northern margin of the EASM (Fig. 6). Lake beach ridges and sediment outcrops, which represent past variations in lake-level elevation and extent (Goldsmith et al., 2017), have been investigated for Lakes Dali and Chagan Nur. The results suggest that, between ~11 and ~5.9–5 ka, lake levels were 12–60 m higher than today (Goldsmith et al., 2017; Li et al., 2020; Fig. 6). A recent study of Lake Gonghai, based on the aquatic origin of branched glycerol dialkyl glycerol tetraethers (brGDGTs), indicated high lake levels during 9.5–5 ka (Cao et al., 2021; Fig. 6). Thus, the concordance of these studies suggests that, within the limits of the available chronologies, high lake levels on the northern margin of the EASM occurred consistently during ~10–5 ka. Furthermore, precipitation reconstructions based on pollen assemblages and biomarkers in lake sediments also show a consistent relationship with lake-level changes (Jiang et al., 2006; Chen et al., 2015; Cao et al. 2021; Fig. 6).

Holocene dust activity on the northern margin of the EASM

EM1 is consistent with the peak at ~0.4 μm of the GSDs for loess deposits in the Chinese Loess Plateau (Yang and Ding, 2004; Fig. 4d). Generally, the very fine component may adhere to the surfaces of large grains, forming aggregates that can be transported by saltation or rolling (Pye, 1995; Derbyshire et al., 1998; Qiang et al., 2010). The fine material may be disaggregated after being deposited in the lake or being treated with ultrasound before grain-size measurements.

EM3 represents the relatively coarse fraction of the Lake Bayanchagan sediments. Its broad peak at ~38 μm (90% within the range of 14–102 μm) (Fig. 4b) is very similar to the dominant mode of coarse loess in the northern part of the Loess Plateau (Sun et al., 2008; Yang and Ding, 2008; Fig. 4d). The consistent variations in EM3 and EM1 suggest that these two portions are transported by wind and can be interpreted as indicators of variations in regional dust sources.

EM4 reflects the coarsest fraction of the Lake Bayanchagan sediments. Its peak at 152 μm (90% within the range of 68–500 μm) (Fig. 4b) is similar to the dominant mode of the
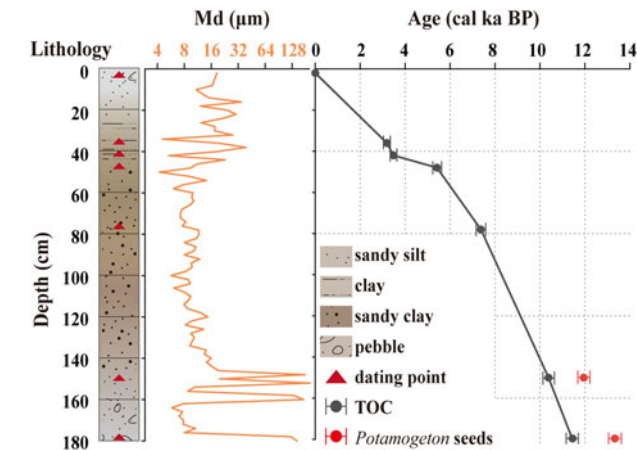

Figure 2. Lithology and median grain-size (Md) data, along with age–depth model data for core BY from Lake Bayanchagan. TOC, total organic carbon.
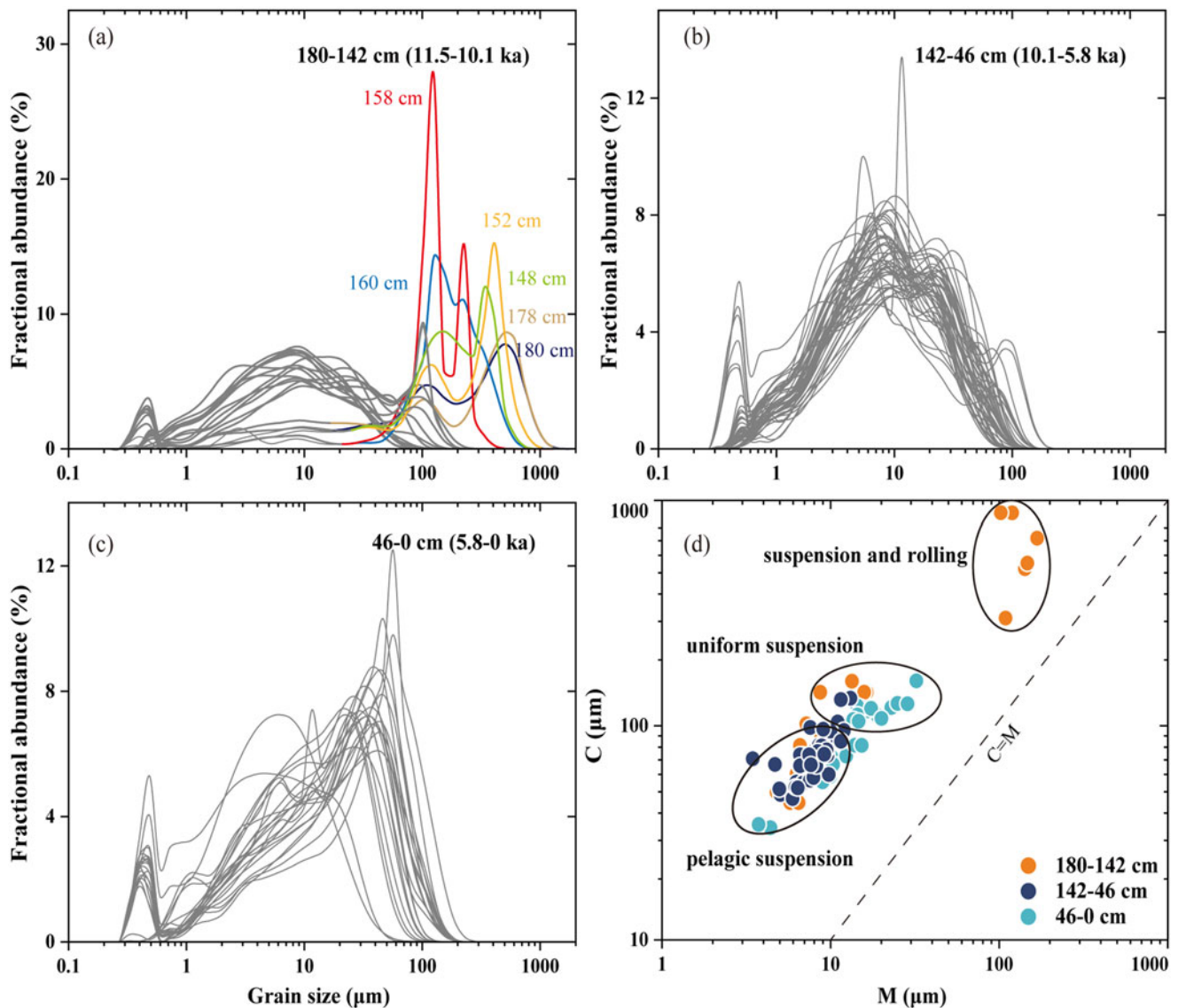
Figure 3. Core BY data. **(a–c)** Grain-size distributions (GSDs). **(d)** C–M plot: C indicates the coarsest percentile of the GSDs (the value at 99%), and M indicates the median (the value at 50%).

nearshore sediments (Guo et al., 2016; Xu et al., 2018; Fig. 4d). Lake Bayanchagan is located within the southern margin of the Otindag Sandy Land (Fig. 1); therefore, EM4 is most likely sourced from local dunes.

The paleoenvironmental record of EM1, EM3, and EM4 within core BY demonstrates that dust activity in the region fluctuated during the 11.5–10 ka interval, while the low values of these three EMs indicate low dust activity during the 10–5.8 ka interval. EM3 increased by ~33% during 5.8–3.8 ka, indicating increased dust activity, which subsequently remained at an overall high level, despite several intervals of low dust activity (Fig. 5).

Dust storm activity is a function of the environmental conditions within the dust source region, including precipitation amount, vegetation cover, and wind strength (Clemens, 1998; Carolin et al., 2019). The major deserts in northern China include the Mu Us Desert, Hobq Desert, Horqin Sandy Land, and Hulunbuir Sandy Land (Fig. 1). All of these deserts are important global dust sources (Dong et al., 1998; Zhang et al., 2018).

Paleoclimatic records indicate that monsoonal precipitation began to increase in the Early Holocene (~11–10 ka) and reached a maximum during ~9–6 ka (Jiang et al., 2006; Chen et al., 2015; Li et al., 2020). Both the vegetation cover and plant diversity gradually increased with this increasing precipitation. During ~11–10 ka, steppe vegetation prevailed, dominated by *Artemisia*, Chenopodiaceae, Poaceae, and *Ephedra*. During 9–6 ka, there was an increase in deciduous broadleaved trees (*Betula*, *Ulmus*, *Quercus*), which were the most diverse plant group throughout the Holocene, together with *Pinus* (Xiao et al., 2004; Jiang et al., 2006; Xu et al., 2010; Wen et al., 2010, 2017; Chen et al., 2015). An increase in the vegetation cover reduces the surface wind strength and increases the soil stability. All these factors, including the increased precipitation and vegetation cover and the decreasing wind strength, led to a large reduction in dust emissions. Therefore, the low dust activity during 10–5.8 ka was likely a response to the humid climate on the northern margin of the EASM. The increased dust activity after 5.8 ka was then
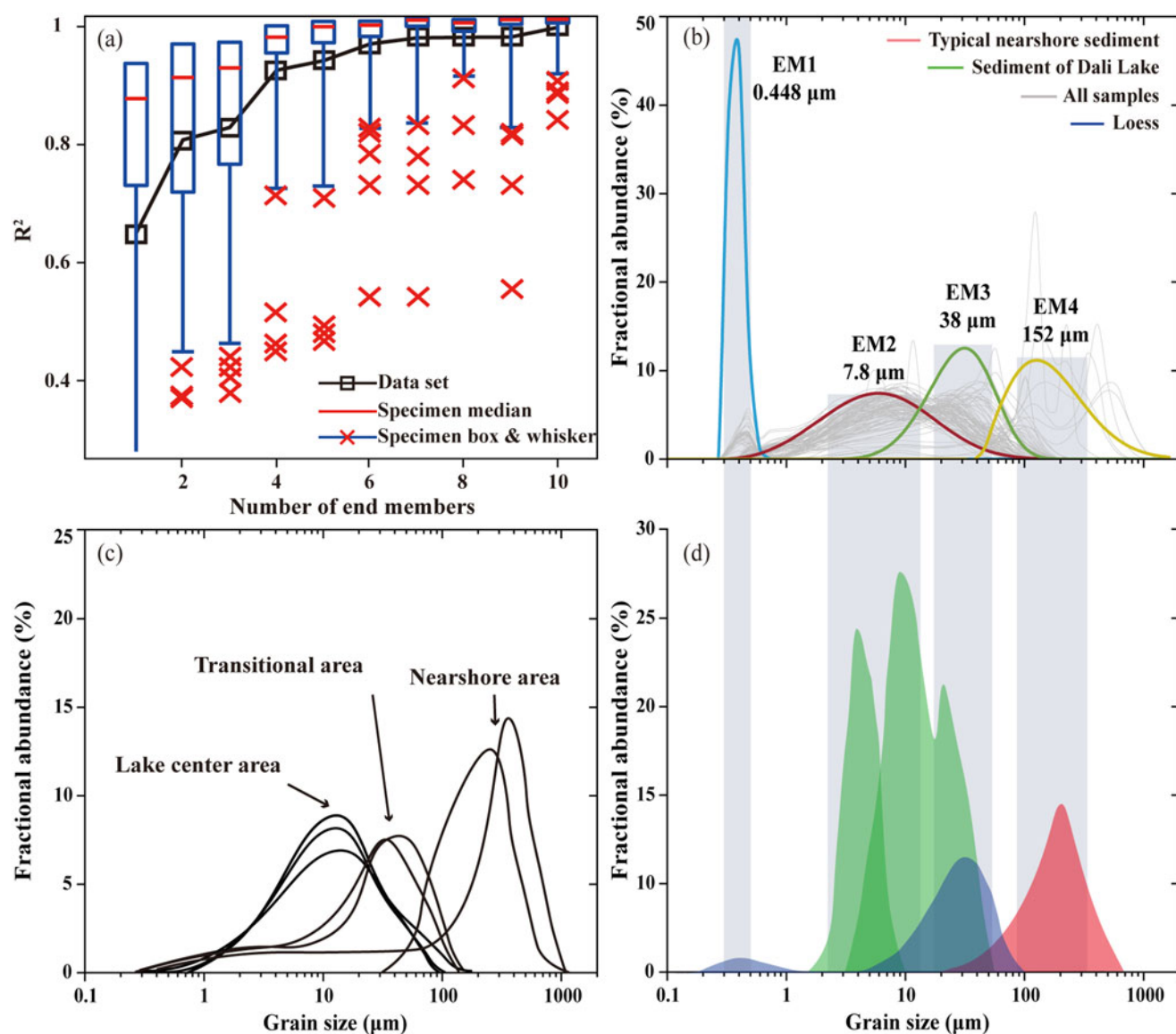
Figure 4. (a) Plot of the coefficient of determination (R^2) versus the number of grain-size endmembers (EMs) chosen to model the observed grain-size distributions (GSDs), from 1 to 10. **(b)** Overlay plot of the GSDs of all samples (n = 90) (gray curves) and the three retained EMs (colored curves). **(c)** Characteristic GSDs of surface sediments collected in the center (left), transitional zone (middle), and nearshore zone (right) of lakes in northern China (modified from Guo et al., 2016). **(d)** Dominant modes of the GSDs of surface sediment samples from the nearshore zone of lakes (red) (Guo et al., 2016; Xu et al., 2018), loess sediments (blue) (Yang and Ding, 2004), and the offshore-suspension component in sediments from Lake Dali (green) (Xiao et al., 2009).
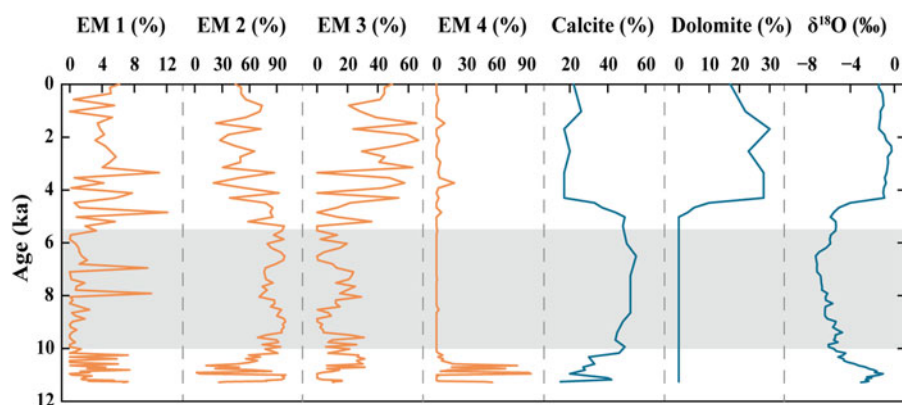

Figure 5. Records of the proportions of EM1, EM2, EM3, EM4, calcite, dolomite, and carbonate $\delta^{18}O$ of core BY. EM, grain-size endmember.
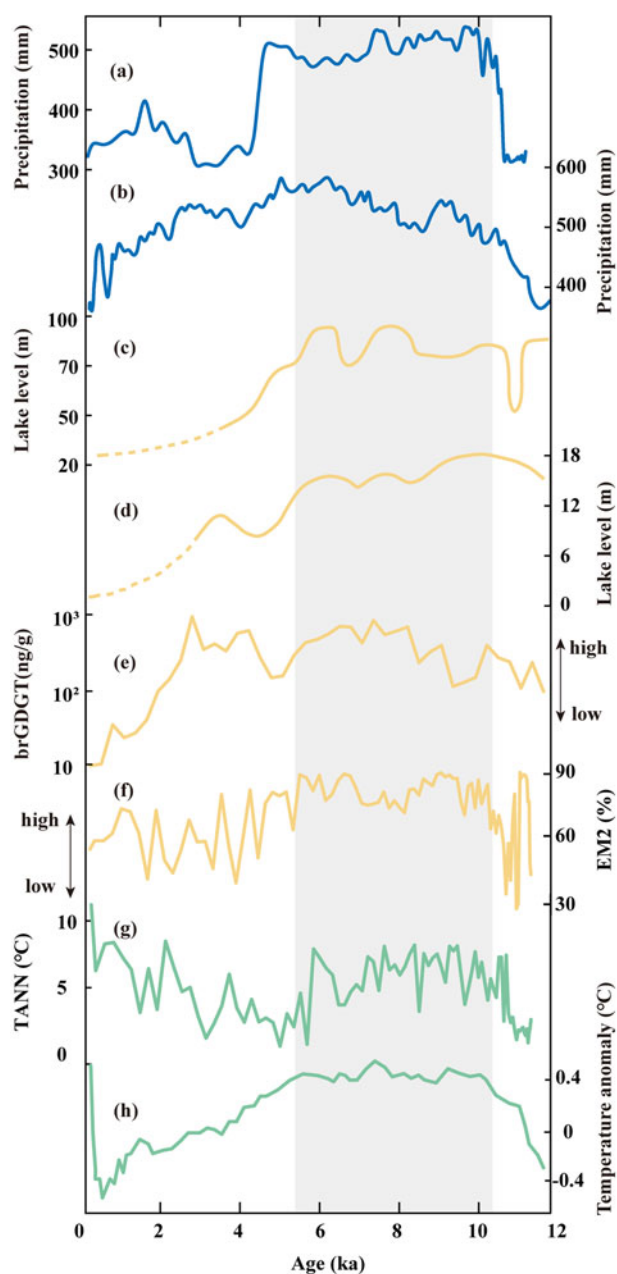
Figure 6. Comparisons of paleoenvironmental records from the northern margin of the EASM and global annual temperature. **(a and b)** Precipitation reconstructed from pollen data from Lake Bayanchagan (Jiang et al., 2006) and Lake Gonghai (Chen et al., 2015). **(c–f)** Lake-level records from Lake Dali (Goldsmith et al., 2017), Lake Chagan Nur (Li et al., 2020), and Lake Gonghai based on branched glycerol dialkyl glycerol tetraether (brGDGT) data (Cao et al., 2021), and Lake Bayanchagan (this study). **(g and h)** Pollen-based temperature reconstruction from Lake Bayanchagan (Jiang et al., 2006) and reconstructed global annual temperature (Marcott et al., 2013). EM2, grain-size endmember 2; TANN, mean annual temperature.

buildup and are associated with enhanced dust activity, whereas paleosol layers indicate dune stabilization, weakened dust activity, and increased vegetation cover (Lu et al., 2011; Xu et al., 2018). Therefore, the eolian sand–paleosol sequences are an archive of changes in the intensity and frequency of paleo-eolian sand activity. A recent study showed that paleosol development in the deserts of northern China started at ~11 ka and that the proportion of vegetation-stabilized dunes gradually increased until ~6 ka (Xu et al., 2020), indicating a trend of decreasing dust activity during 11–6 ka. After ~6–5 ka, the reduction of the proportion of vegetation-stabilized dunes, as well as less frequent and thinner paleosols, indicate dune reactivation (Yang et al., 2011; Lu et al., 2013; Xu et al. 2020), which is consistent with our inference of intensified dust emissions.

Holocene lake high stands on the northern margin of the EASM region

Our study has illustrated that the high stand of Lake Bayanchagan corresponded to the interval of high monsoon precipitation and low dust activity during the ~10–5.8 ka interval, in accord with other paleoclimatic records from the northern margin of the EASM (Goldsmith et al., 2017; Xu et al., 2018; Li et al., 2020). The temperature in northern China during this interval increased by ~2–4°C (Jiang et al., 2006; Zhang et al., 2022; Fig. 6), suggesting that, during ~10–6 ka, high precipitation occurred synchronously with high temperatures across northern China. Geological records and climate simulations show that the displacement of the EASM rain belt is associated with the migration of the Intertropical Convergence Zone (ITCZ), which moved northward in response to pronounced Northern Hemisphere warming during the mid-Holocene (Yang et al. 2015, 2019; Huang et al., 2021; Sun et al., 2022). This led to the northward shift of the monsoonal rain belt, causing a widespread increase in precipitation, which in turn resulted in lake high stands on the northern margin of the EASM. As global warming continues, the northern margin of the EASM is projected to become wetter, and dust storm activity will be weakened (Yang et al. 2015; Huang et al., 2021).

CONCLUSIONS

We used a high-resolution grain-size record, along with carbonate mineralogy, from sediments of Lake Bayanchagan on the northern margin of the EASM to reconstruct changes in lake level and dust activity over the past 11.5 ka. The results show that the level of Lake Bayanchagan was relatively low during 11.5–10.8 ka, and that then it gained water during ~10.8–10 ka. The high stand of Lake Bayanchagan and low level of dust activity occurred during ~10–5.8 ka. After 5.8 ka, the lake level decreased, corresponding to increased dust activity. The strong similarity between the carbonate $\delta^{18}O$ and grain-size records of Lake Bayanchagan, together with the variations of sedimentary calcite and dolomite contents, indicate that the lake-level fluctuations of Lake Bayanchagan during the Holocene were driven by changes in monsoonal precipitation. A regional comparison suggests that lake-level high stands and high precipitation values occurred synchronously on the northern margin of the EASM during ~10 to ~6 ka, corresponding to the Holocene thermal maximum. At this time, the ITCZ had moved northward in response to this significant climatic warming, driving a northwestward shift of the EASM rain belt and enhanced monsoonal rainfall. After 5.8 ka,

related to large-scale drought conditions and the associated vegetation degradation caused by the decrease in monsoonal precipitation.

The stratigraphy in deserts is characterized by the alternation of eolian sand layers and paleosols. These alternating sequences cover an area of ~10^5 km^2 in the deserts located to the east of the Helan Mountains (Zhang et al., 2018; Fig. 1). Eolian sand layers represent periods of dune-field expansion and/or dune

the ITCZ had migrated southward due to the decreasing temperatures, leading to a southeastward shift of the EASM rain belt and decreased monsoonal precipitation. This climatic change was associated with extensive drought conditions, falling lake levels, and enhanced dust activity.

REFERENCES

An, Z., Porter, S.C., Kutzbach, J.E., Wu, X., Wang S., Liu,., Li, X., Zhou, W., 2000. Asynchronous Holocene optimum of the East Asian monsoon. *Quaternary Science Reviews* **19**, 743–762.

Bravard, J., Goichot, M., Tronchère, H., 2014. An assessment of sediment-transport processes in the Lower Mekong River based on deposit grain sizes, the CM technique and flow-energy data. *Geomorphology* **207**, 174–189.

Cao, J., Rao, Z., Shi, F., Lian, E., Jia, G., 2021. Lake-level records support a mid-Holocene maximum precipitation in northern China. *Science China Earth Sciences* **64**, 2161–2171.

Carolin, S., Walker, R., Day, C., 2019. Precise timing of abrupt increase in dust activity in the Middle East coincident with 4.2 ka social change. *Proceedings of the National Academy of Sciences USA* **116**, 67–72.

Chen, F., Chen, S., Zhang, X., Chen, J., Wang, X., Gowan, E. J., Qiang, M., et al., 2020. Asian dust-storm activity dominated by Chinese dynasty changes since 2000 BP. *Nature Communications* **11**, 992.

Chen, F., Qiang, M., Zhou, A., Xiao, S., Chen, J., Sun, D., 2013. A 2000-year dust storm record from Lake Sugan in the dust source area of arid China. *Journal of Geophysical Research: Atmospheres* **118**, 2149–2160.

Chen, F., Xu, Q., Chen, J., 2015. East Asian summer monsoon precipitation variability since the last deglaciation. *Scientific Reports* **5**, 11186.

Clemens, S., 1998. Dust response to seasonal atmospheric forcing: Proxy evaluation and calibration. *Paleoceanography* **13**, 471–490.

Derbyshire, E., Meng, X., Kemp, R.A., 1998. Provenance, transport and characteristics of modern aeolian dust in western Gansu Province, China, and interpretation of the Quaternary loess record. *Journal of Arid Environments* **39**, 497–516.

Dietze, E., Maussion, F., Ahlborn, M., 2014. Sediment transport processes across the Tibetan Plateau inferred from robust grain-size end members in lake sediments. *Climate of the Past* **10**, 91–106.

Ding, Z.L., Derbyshire, E., Yang, S.L., Sun, J.M., Liu, T.S., 2005. Stepwise expansion of desert environment across northern China in the past 3.5 Ma and implications for monsoon evolution. *Earth and Planetary Science Letters* **237**, 45–55.

Dong, G., Wang, G., Li, X., 1998. Palaeomonsoon vicissitudes in eastern desert region of China since last interglacial period. [In Chinese with English abstract.] *Science China Earth Sciences* **41**, 215–224.

Goldsmith, Y., Broecker, W.S., Xu, H., Polissar, P.J., deMenocal, P.B., Porat, N., Lan, J., Cheng, P., Zhou, W., An, Z., 2017. Northward extent of East Asian monsoon covaries with intensity on orbital and millennial timescales. *Proceedings of the National Academy of Sciences USA* **114**, 1817–1821.

Gu, N., Jiang, W., Wang, L., Zhang, E., Yang, S., Xiong, S., 2015. Rainfall thresholds for the precipitation of carbonate and evaporite minerals in modern lakes in northern China. *Geophysical Research Letters* **42**, 5895–5901.

Guo, X., Wang, W., Wang, G., Liu, L., Ma, Y., Jiang, H.E., 2016. Within-lake distributions of grain-size components and environmental implications based on the survey of lake surface sediment of Chinese monsoon marginal area. [In Chinese with English abstract.] *Geographical Research* **35**, 677–691.

Håkanson, L., Jansson, M., 1983. *Principles of Lake Sedimentology*. Springer, Berlin.

Held, I.M., Soden, B.J., 2006. Robust responses of the hydrological cycle to global warming. *Journal of Climate* **19**, 5686–5699.

Hou, J., D'Andrea, W.J., Liu, Z., 2012. The influence of ^{14}C reservoir age on interpretation of paleolimnological records from the Tibetan Plateau. *Quaternary Science Reviews* **48**, 67–79.

Huang, X., Yang, S., Haywood, A., Jiang, D., Wang, Y., Sun, M., Tang, Z., Ding, Z., 2021. Warming-induced northwestward migration of the Asian summer monsoon in the geological past: evidence from climate simulations and geological reconstructions. *Journal of Geophysical Research: Atmospheres* **126**, e2021JD035190.

Jiang, W., Guo, Z., Sun, X., Wu, H., Chu, G., Yuan, B., Hatté, C., Guiot, J., 2006. Reconstruction of climate and vegetation changes of Lake Bayanchagan (Inner Mongolia): Holocene variability of the East Asian monsoon. *Quaternary Research* **65**, 411–420.

Jiang, W., Liu, T., 2007. Timing and spatial distribution of mid-Holocene drying over northern China: response to a south-eastward retreat of the East Asian monsoon. *Journal of Geophysical Research: Atmospheres* **112**, D24111.

Leng, M., Marshall, J., 2004. Palaeoclimate interpretation of stable isotope data from lake sediment archives. *Quaternary Science Reviews* **23**, 811–831.

Lerman, A., 1978. *Lakes: Chemistry, Geology, Physics*. Springer-Verlag, New York.

Li, G., Wang, Z., Zhao, W., Jin, M., Wang, X., Tao, S., Chen, C., et al., 2020. Quantitative precipitation reconstructions from Chagan Nur revealed lag response of East Asian summer monsoon precipitation to summer insolation during the Holocene in arid northern China. *Quaternary Science Reviews* **239**, 106365.

Li, Y., Song, Y., Qiang, M., Miao, Y., Zeng, M., 2019. Atmospheric dust variations in the Ili Basin, northwest China, during the last glacial period as revealed by a high mountain loess-paleosol sequence. *Journal of Geophysical Research: Atmospheres* **124**, 8449–8466.

Liu, T.S., 1985. *Loess and the Environment*. China Ocean Press, Beijing.

Liu, X., Vandenberghe, J., An, Z., Li, Y., Jin, Z., Dong, J., Sun, Y., 2016. Grain size of Lake Qinghai sediments: implications for riverine input and Holocene monsoon variability. *Palaeogeography, Palaeoclimatology, Palaeoecology* **449**, 41–51.

Lu, H., Mason, J., Stevens, T., 2011. Response of surface processes to climatic change in the dunefields and Loess Plateau of North China during the late Quaternary. *Earth Surface Processes and Landforms* **36**, 1590–1603.

Lu, H., Yi, S., Xu, Z., 2013. Chinese deserts and sand fields in last glacial maximum and Holocene optimum. *Chinese Science Bulletin* **58**, 2775–2783.

Marcott, A., Shakun Jeremy, D., Clark Peter, U., Mix Alan, C., 2013. A reconstruction of regional and global temperature for the past 11,300 years. *Science* **339**, 1198–1201.

Meyer, I., Davies, G.R., Vogt, C., Kuhlmann, H., Stuut, J.-B.W., 2013. Changing rainfall patterns in NW Africa since the Younger Dryas. *Aeolian Research* **10**, 111–123.

Meyer, I., Van Daele, M., Tanghe, N., De Batist, M., Verschuren, D., 2020. Reconstructing East African monsoon variability from grain-size distributions: end-member modeling and source attribution of diatom-rich sediments from Lake Chala. *Quaternary Science Reviews* **247**, 106574.

Müller, G., Irion, G., Förstner, U., 1972. Formation and diagenesis of inorganic Ca-Mg carbonates in the lacustrine environment. *Naturwissenschaften* **59**, 158–164.

Olsson, I.U., 2009. Radiocarbon dating history: early days, questions, and problems. *Radiocarbon* **51**, 1–43.

Passega, R., 1964. Grain size representation by CM patterns as a geological tool. *Journal of Sedimentary Petrology* **34**, 830–847.

Paterson, G.A., Heslop, D., 2015. New methods for unmixing sediment grain size data. *Geochemistry, Geophysics, Geosystems* **16**, 4494–4506.

Peng, Y., Xiao, J., Nakamura, T., Liu, B., Inouchi, Y. 2005. Holocene East Asian monsoonal precipitation pattern revealed by grain-size distribution of core sediments of Daihai Lake in Inner Mongolia of north-central China. *Earth and Planetary Science Letters* **233**, 467–479.

Pye, K., 1995. The nature, origin and accumulation of loess. *Quaternary Science Reviews* **14**, 653–667.

Qiang, M., Lang, L., Wang, Z., 2010. Do fine-grained components of loess indicate westerlies: Insights from observations of dust storm deposits at Lenghu (Qaidam Basin, China). *Journal of Arid Environments* 74, 1232–1239.

Qiang, M., Liu, Y., Jin, Y., Song, L., Huang, X., Chen, F., 2014. Holocene record of eolian activity from Genggahai Lake, northeastern Qinghai-Tibetan Plateau, China. *Geophysical Research Letters* 41, 589–595.

Renssen, H., Seppä, H., Crosta, X., Goosse, H., Roche, D.M., 2012. Global characterization of the Holocene Thermal Maximum. *Quaternary Science Reviews* 48, 7–19.

Shapley, M.D., Ito, E., Donovan, J.J., 2005. Authigenic calcium carbonate flux in groundwater-controlled lakes: implications for lacustrine paleoclimate records. *Geochimica et Cosmochimica Acta* 69, 2517–2533.

Shi, F., Lu, H., Guo, Z., Yin, Q., Wu, H., Xu, C., Zhang, E., et al., 2021. The position of the current warm period in the context of the past 22,000 years of summer climate in China. *Geophysical Research Letters* 48, e2020GL091940.

Sun, D., Su, R., Bloemendal, J., Lu, H., 2008. Grain-size and accumulation rate records from Late Cenozoic aeolian sequences in northern China: implications for variations in the East Asian winter monsoon and westerly atmospheric circulation. *Palaeogeography, Palaeoclimatology, Palaeoecology* 264, 39–53.

Sun, M., Yang, S., Xiao, J., Wang, Y., Huang, X., Zhang, S., Yang, X., Jiang, W., Ding, Z., 2022. BrGDGTs-based temperature and hydrological reconstruction from fluvio-lacustrine sediments in the monsoonal North China Plain since 31 kyr BP. *Quaternary Science Reviews* 277, 107268.

Stuiver, M., Reimer, P.J., 1993. Extended ^{14}C data base and revised CALIB 3.0 ^{14}C age calibration program. *Radiocarbon* 35, 215–230.

Stuiver, M., Reimer, P.J. Reimer, R.W., 2020. CALIB 8.2. http://calib.org.

Talbot, M.R., Allen, P.A., 1996, Lakes. In: Reading, H.G. (Ed.), *Sedimentary Environments: Processes, Facies and Stratigraphy.* Blackwell Science, Oxford, pp. 5–36.

Törnqvist, T.E., De Jong, A.F.M., Oosterbaan, W.A., Van Der Borg, K., 1992. Accurate dating of organic deposits by AMS ^{14}C measurement of macrofossils. *Radiocarbon* 34, 566–577.

Wang, W., Lee, X., Xiao, W., Liu, S., Schultz, N., Wang, Y., Zhang, M., Zhao, L., 2018. Global lake evaporation accelerated by changes in surface energy allocation in a warmer climate. *Nature Geoscience* 11, 410–414.

Wen, R., Xiao, J., Chang, Z., Zhai, D., Xu, Q., Li, Y., Itoh, S., Lomtatidze, Z., 2010. Holocene climate changes in the mid-high-latitude-monsoon margin reflected by the pollen record from Hulun Lake, northeastern Inner Mongolia. *Quaternary Research* 73, 293–303.

Wen, R., Xiao, J., Fan, J., Zhang, S., Yamagata, H., 2017. Pollen evidence for a mid-Holocene East Asian summer monsoon maximum in northern China. *Quaternary Science Reviews* 176, 29–35.

Xiao, J., Chang, Z., Si, B., Qin, X., Itoh, S., Lomtatidze, Z., 2009. Partitioning of the grain-size components of Dali Lake core sediments: evidence for lake-level changes during the Holocene. *Journal of Paleolimnology* 42, 249–260.

Xiao, J., Xu, Q., Nakamura, T., Yang, X., Liang, W., Inouchi, Y., 2004. Holocene vegetation variation in the Daihai Lake region of north-central China: a direct indication of the Asian monsoon climatic history. *Quaternary Science Reviews* 23, 1669–1679.

Xu, B., Wang, L., Gu, Z., Hao, Q., Wang, H., Chu, G., Jiang, D., Liu, Q., Qin, X., 2018. Decoupling of climatic drying and Asian dust export during the Holocene. *Journal of Geophysical Research: Atmospheres* 123, 915–928.

Xu, Q., Xiao, J., Li, Y., Tian, F., Nakagawa, T., 2010. Pollen-based quantitative reconstruction of Holocene climate changes in the Daihai Lake area, Inner Mongolia, China. *Journal of Climate* 23, 2856–2868.

Xu, Z., Mason, J.A., Xu, C., Yi, S., Bathiany, S., Yizhaq, H., Zhou, Y., Cheng, J., Holmgren, M., Lu, H., 2020. Critical transitions in Chinese dunes during the past 12,000 years. *Science Advances* 6, eaay8020.

Yang S., Ding Z., 2004. Comparison of particle size characteristics of the Tertiary "red clay" and Pleistocene loess in the Chinese Loess Plateau: implications for origin and sources of the "red clay." *Sedimentology* 51, 77–93.

Yang, S., Ding, Z., 2008. Advance-retreat history of the East-Asian summer monsoon rainfall belt over northern China during the last two glacial-interglacial cycles. *Earth and Planetary Science Letters* 274, 499–510.

Yang, S., Ding, Z., Li, Y., Wang, X., Jiang, W., Huang, X., 2015. Warming-induced northwestward migration of the East Asian monsoon rain belt from the Last Glacial Maximum to the mid-Holocene. *Proceedings of the National Academy of Sciences USA* 112, 13178–13183.

Yang, S., Ding, Z., Wang, X., Tang, Z., Gu, Z., 2012. Negative δ^{18}O-δ^{13}C relationship of pedogenic carbonate from northern China indicates a strong response of C_3/C_4 biomass to the seasonlity of Asian monsoon precipitation. *Palaeogeography, Palaeoclimatology, Palaeoecology* 317/318, 32–40.

Yang, S., Dong, X., Xiao, J., 2019. The East Asian monsoon since the last glacial maximum: evidence from geological records in northern China. *Science China Earth Sciences* 62, 1181–1192.

Yang, X., Scuderi, L., Paillou, P., 2011. Quaternary environmental changes in the drylands of China—a critical review. *Quaternary Science Reviews* 30, 3219–3233.

Zhang, C., Shen, Y., Li, Q., Jia, W., Li, J., Wang, X., 2018. Sediment grain-size characteristics and relevant correlations to the aeolian environment in China's eastern desert region. *Science of the Total Environment* 627, 586–599.

Zhang, P., Jeong, J.-H., Yoon, J.-H., Kim, H., Wang, S.Y.S., Linderholm, H.W., Fang, K., Wu, X., Chen, D., 2020. Abrupt shift to hotter and drier climate over inner East Asia beyond the tipping point. *Science* 370, 1095–1099.

Zhang, W., Wu, H., Cheng, J., Geng, J., Li, Q., Sun, Y., Yu, Y., Lu, H., Guo, Z., 2022. Holocene seasonal temperature evolution and spatial variability over the Northern Hemisphere landmass. *Nature Communications* 13: 5334.

Zhou, J., Wu, J., Ma, L., Qiang, M., 2019. Late Quaternary lake-level and climate changes in arid central Asia inferred from sediments of Ebinur Lake, Xinjiang, northwestern China. *Quaternary Research* 92, 416–429.